









Cite this: *Nanoscale Adv.*, 2020, 2, 3017

# A magnetic immunoconjugate nanoplatform for easy colorimetric detection of the NS1 protein of dengue virus in infected serum

Ramsés Ramírez-Navarro, <sup>a</sup> Peter Polesnak, <sup>b</sup> Julio Reyes-Leyva, <sup>c</sup>  
Ubydul Haque, <sup>d</sup> Juan Carlos Vazquez-Chagoyán, <sup>e</sup> Martín R. Pedroza-  
Montero, <sup>f</sup> Miguel A. Méndez-Rojas <sup>\*b</sup> and Aracely Angulo-Molina <sup>\*af</sup>

In this work, as a proof of principle, the design and performance evaluation of a simple, cheap and efficient colorimetric test for the detection of the NS1 protein of dengue virus, assisted by an immunoconjugate of magnetite (Fe<sub>3</sub>O<sub>4</sub>) nanoparticles coupled to anti-NS1 antibodies is reported. A monoclonal antibody against the NS1 antigen was covalently immobilized on the surface of superparamagnetic iron oxide nanoparticles (SPIONs ~ 20 nm) and used for the immunodetection of this protein. When the magnetic immuno-nanoplatform is added into infected serum, it conjugates with the NS1 protein and can then be easily separated using an external magnetic field; then, the recovered immunoconjugate is transferred into a well containing a second immobilized NS1-antibody to form an ELISA-type system. When the NS1 protein is present, a color change to blue is induced by reaction with the Perls reagent, which is consistent with the formation of a SPION-antibody-NS1 antigen-antibody conjugate that confirms infection. No false positives were found when NS1 was not present or a different antibody and the NS1 protein were added into the system. The experimental findings could be extrapolated and scaled up to lead to future developments of simple, quick, and inexpensive, *in situ* biomolecular diagnostic tests for emergent viral infections.

Received 30th March 2020  
Accepted 18th May 2020

DOI: 10.1039/d0na00251h

rsc.li/nanoscale-advances

## Introduction

Dengue fever is mainly caused by the female mosquito *Aedes aegypti* and presents four virus serotypes (DENV1–DENV4). One-third of the world's population is at risk, as the disease is endemic in 128 countries; each year, up to 400 million people get infected with dengue. Around 100 million people get sick from infection, and 22 000 die from severe dengue.<sup>1,2</sup> The disease is widespread throughout the tropics and subtropical areas, influenced strongly by rainfall and temperature and, in the last few

years, by climate change. In Latin America, we can find the four dengue serotypes DENV1, DENV2, DENV3 and DENV4 with hyperendemic patterns.<sup>3</sup> In Mexico, 41 505 cases were confirmed during 2019, with 13 261 cases showing strong and severe symptoms.<sup>4</sup> These data do not include infected persons who did not go to a health center, or who may be mis-diagnosed with other diseases, in which case death of the individual may occur as a consequence of lack of appropriate medical treatment. The incidence, spread and severity of dengue disease have increased worldwide. For this reason, a timely diagnosis of this disease is highly important for the appropriate handling of the patient.<sup>2–5</sup>

In the case of viral infectious diseases such as dengue and others, early identification would allow a rapid response and adequate clinical treatment, thus offering greater possibilities for recovery.<sup>6</sup> Currently the diagnosis of dengue is made through the PCR technique, this being considered the gold standard or preferred choice. This analytical technique has the ability to detect and differentiate between the different serotypes of the virus, but its high cost associated with the use of specialized equipment and the need of being performed in analytical laboratories represent a serious limitation. Likewise, serological tests have been implemented which detect viral proteins such as the NS1 protein, which can be found shortly in the body fluids of the patient after infection; the blood values of NS1 range from several ng mL<sup>-1</sup> to several µg mL<sup>-1</sup> and peaked

<sup>a</sup>Departamento de Ciencias Químico Biológicas, Universidad de Sonora (UNISON), Luis Encinas y Rosales S/N, Col. Centro, 83000, Hermosillo, Sonora, México. E-mail: aracely.angulo@unison.mx

<sup>b</sup>Departamento de Ciencias Químico-Biológicas, Universidad de las Américas Puebla, Ex-Hacienda de Santa Catarina Mártir, 72820, San Andrés Cholula, Puebla, México. E-mail: miguela.mendez@udlap.mx

<sup>c</sup>Centro de Investigación Biomédica de Oriente, Instituto Mexicano del Seguro Social, Metepec, 74360, Atlixco, Puebla, México

<sup>d</sup>Department Biostatistics and Epidemiology, University of North Texas Health Science Center, Fort Worth, Texas, USA

<sup>e</sup>Centro de Investigación y Estudios Avanzados en Salud Animal, Facultad de Medicina Veterinaria y Zootecnia, Universidad Autónoma del Estado de México, Toluca, Estado de México, México

<sup>f</sup>Departamento de Investigación en Física, DIFUS, Universidad de Sonora (UNISON), Luis Encinas y Rosales S/N, Col. Centro, 83000, Hermosillo, Sonora, México



at  $50 \mu\text{g mL}^{-1}$  of serum in acute cases, often reported in the literature. However, this range depends on several factors, such as the progression of the infection,<sup>7</sup> virus serotype,<sup>8</sup> immunologic stage<sup>9</sup> and primary or secondary infections.<sup>10</sup> Taking into account all data reported until today, the operating range of NS1 detection in serum to design an useful diagnostic tool will be required to go from  $\text{ng mL}^{-1}$  to  $\mu\text{g mL}^{-1}$ . NS1 is a highly conserved protein in the virus and is one of the seven non-structural proteins encoded by dengue virus genome. NS1 presents the ability to bind to IgG and IgM antibodies expressed upon its presence. In conventional serological tests, NS1 presents problems in detection specificity, in addition to a loss of sensitivity in the early stages of infection.<sup>11,12</sup>

Recently, the use of magnetic iron oxide nanoparticles, such as magnetite, as a nanoplatform has attracted the attention of several research groups around the world due to its potential biomedical applications. Since the small sized iron oxide NPs have a large surface area, they will present several available sites for the conjugation of useful biomedical molecules such as antibodies. Also, the physical properties of nanomaterials, such as magnetism, electronic structure and optical properties, can be easily tuned and modified.<sup>13,14</sup> It has been recently found that the sensitivity for the detection of certain molecules associated with viral or bacterial infections can be enhanced using metallic NPs.<sup>15,16</sup> Also, as exogenous iron oxide NPs can be detected in tissues and other major organs using the Perls reagent which upon reaction produces a blue precipitate, this reaction can be useful for the colorimetric detection of iron oxide NPs. Considering the above, in this work the development of a cheap magnetic immunoconjugate nanoplatform for the colorimetric detection of the NS1 dengue protein, using NS1 antibodies covalently attached to the surface of magnetite nanoparticles, is reported. For clinical purposes, the system here developed is able to detect positive samples of NS1 even if is the first time of infection or it is a reinfection. This method could be used in areas with resource-scarce settings, and it may be easily adapted for the detection of proteins associated with other emerging viral infections, such as the current SARS-Cov-2 pandemic.

## Experimental section

### Materials

All the reagents were of analytical grade and used without further purification. Ferrous chloride tetrahydrate ( $\text{FeCl}_2 \cdot 4\text{H}_2\text{O}$ , Cat: 2202997, Lot: MKBJ2807, 98%, Aldrich), and ferric chloride hexahydrate ( $\text{FeCl}_3 \cdot 6\text{H}_2\text{O}$ ) salts, as iron(II) and iron(III) precursors, with a solution of 25% ammonium hydroxide ( $\text{NH}_4\text{OH}$ , Cat: 221228, Lot: SHBG1201V, 28–30%, Aldrich), sodium citrate as a stabilizer ( $\text{Na}_3\text{C}_6\text{H}_5\text{O}_7$ , Cat: 54641, Lot: SLBM1808V, 99%, Aldrich), anhydrous toluene (Cat: 244511, Lot: SHBC9582V, 99.8%, Aldrich) and (3-aminopropyl)trimethoxysilane (APTMS,  $\text{H}_2\text{N}(\text{CH}_2)_3\text{Si}(\text{OCH}_3)_3$ , Cat: 281778, Lot: BCBL6126V, 97%, Aldrich), were purchased from commercial sources and used as received if not otherwise indicated.

### Synthesis of $\text{Fe}_3\text{O}_4$ NPs

Magnetite ( $\text{Fe}_3\text{O}_4$ ) nanoparticles were prepared by the coprecipitation method, as previously described in the literature.<sup>17,18,21</sup> In summary, 1.23 g (4.56 mmol) of  $\text{FeCl}_2 \cdot 6\text{H}_2\text{O}$  and 0.557 g (2.28 mmol) of  $\text{FeCl}_3 \cdot 4\text{H}_2\text{O}$  were mixed, with a molar ratio of 2 : 1 in 8.0 mL of triple-distilled water under intense agitation. The mixture was heated at  $60^\circ\text{C}$  and stirred for 30 minutes. Then, 2.0 mL of a 25%  $\text{NH}_4\text{OH}$  solution was added, and 5 minutes later, 500.0  $\mu\text{L}$  of a sodium citrate solution at a concentration of 500.0  $\text{mg mL}^{-1}$  was added. The solution was left for 60 minutes, under the same heating and reflux conditions. The black precipitate was magnetically decanted using a Nd magnet and washed with triple-distilled water (three times) and ethanol in a 1 : 1 ratio and then separated by magnetic decantation. Finally, the black solid was dried under vacuum at 80 kPa, at  $60^\circ\text{C}$ , for 16 hours.<sup>17,18,21</sup>

### Functionalization of $\text{Fe}_3\text{O}_4$ NPs

50.0 mg of recently prepared and dried  $\text{Fe}_3\text{O}_4$  NPs were re-dispersed in 15.0 mL of anhydrous toluene, and mixed with 35.0  $\mu\text{L}$  of APTMS at  $60^\circ\text{C}$  for 4 hours under stirring. After this, the product was magnetically separated and washed with toluene to eliminate residual APTMS not coupled to the nanoparticles. Then, the product was dried under vacuum conditions (80 kPa), at  $60^\circ\text{C}$  for 16 hours, to avoid oxidation.<sup>19</sup>

### Nanoparticle characterization

To determine the size distribution and hydrodynamic diameter of the NPs, a Nano-Flex Serial W3298 (Microtrac) dynamic light scattering (DLS) instrument was used.<sup>14</sup> The morphology of the NPs was analyzed with a Nova Nano SEM 200 Mark (FEI) field emission STEM (scanning transmission electron microscopy) instrument, working at 30 kV.<sup>20</sup> The presence of functional groups of silanized NPs was determined using a Cary 630 (Agilent Technologies) Fourier transform infrared (FTIR) spectrophotometer, with a spectral window from  $4000 \text{ cm}^{-1}$  to  $400 \text{ cm}^{-1}$ .<sup>21,22</sup>

### Cell culture

The U937-DC-SIGN cell line (ATCC® CRL-3253™) was cultured in the RPMI-1640 medium supplemented with 5% fetal bovine serum (FBS) and incubated at  $37^\circ\text{C}$  and 5%  $\text{CO}_2$ .

### Production of protein NS1

A suspension of cell line U937-DC-SIGN was prepared in 2.0 mL of the RPMI medium without serum and 1.0 mL of the suspension was placed in two conical tubes. One of the tubes was treated with 5.0  $\mu\text{L}$  of a virus inoculum (DENV2), at a concentration of  $6 \times 10^8$  PFU  $\text{mL}^{-1}$  (1 MOI). They were incubated for one hour and then centrifuged at 1000 rpm for 5 min, eliminating the supernatant. It was resuspended in 3.0 mL of RPMI at 5% SFB, to achieve a concentration of 1 000 000 cells per mL. After 24 hours of incubation, it was centrifuged at 3500 rpm for 5 min, recovering the control and infected supernatant. The total protein in the supernatant was



quantified using the Bradford 1X Dye Reagent Quick Start™ reagent (Cat: 500-0205, Lot: 200005735, BIO-RAD), and by reading its absorbance at 570 nm. The infected supernatant and the control supernatant were analyzed.<sup>23</sup> In addition, to determine the presence of the NS1 protein, an electrophoretic profile analysis was performed. Therefore, 12% SDS-PAGE was performed under reducing, non-denaturing conditions. The gels were 0.75 mm thick and loaded with 35.0 μg of the protein. The run was carried out at 100 volts per 90 minutes, and then dyed using Coomassie Blue.<sup>24</sup> The banding profile and the relative abundance were obtained using a photo-document (XR + Imaging System, Gel Doc, Molecular Imager, BIO-RAD).

### Nanopatform design for the detection of the NS1 protein

**Formation of the conjugate Fe<sub>3</sub>O<sub>4</sub> NPs – Ab.** To prepare the nanoparticle-antibody conjugate, 4.0 mg of silanized NPs were resuspended in 1.0 mL of 1X PBS, stirred until dissolved and sonicated for 10 min. The antibody Ab41616 (ms mAb [DN2] dengue virus NS1 glycoprotein antibody, Lot: GR256259-1, ABCAM, stock concentration 0.705 mg mL<sup>-1</sup>) was diluted to 1 : 30. We evaluated different volumes of the antibody (20.0,

40.0 & 60.0 μL corresponding to 0.47, 0.94 & 1.41 μg mL<sup>-1</sup> respectively) to be added in the NPs for its conjugation to know the optimum concentration. The interaction was carried out for one hour at room temperature, with occasional movement. After the incubation, 3 washes were performed, decanting magnetically and resuspending in 1.0 mL of PBS 1X. The conjugate was kept refrigerated at 4 °C until use.<sup>25</sup>

**Preparation of microplates.** The bottoms of 96-well plates (biologend B211303) were coated with 100 μL of the first antibody Ab42316 (ms mAb [DN2] dengue virus NS1 glycoprotein antibody Lot: GR280343-1, ABCAM) diluted to 1 : 30 and incubated for 24 hours at 4 °C. Then, the remaining available anchoring sites on the plates were blocked with 100.0 μL of a blocking solution containing 5% albumin in each well, allowed to incubate for 1 hour, and subsequently washed 6 times with PBS 1X.<sup>18</sup>

**Recognition of the NS1 protein.** For this purpose, 100.0 μL of 24 hour supernatants of the infected U937-DC-SIGN line and controls diluted to 1 : 5 were added into the wells. The plates were incubated for 1 hour at room temperature. After incubation, the wells were washed with PBS 1X.<sup>25</sup>

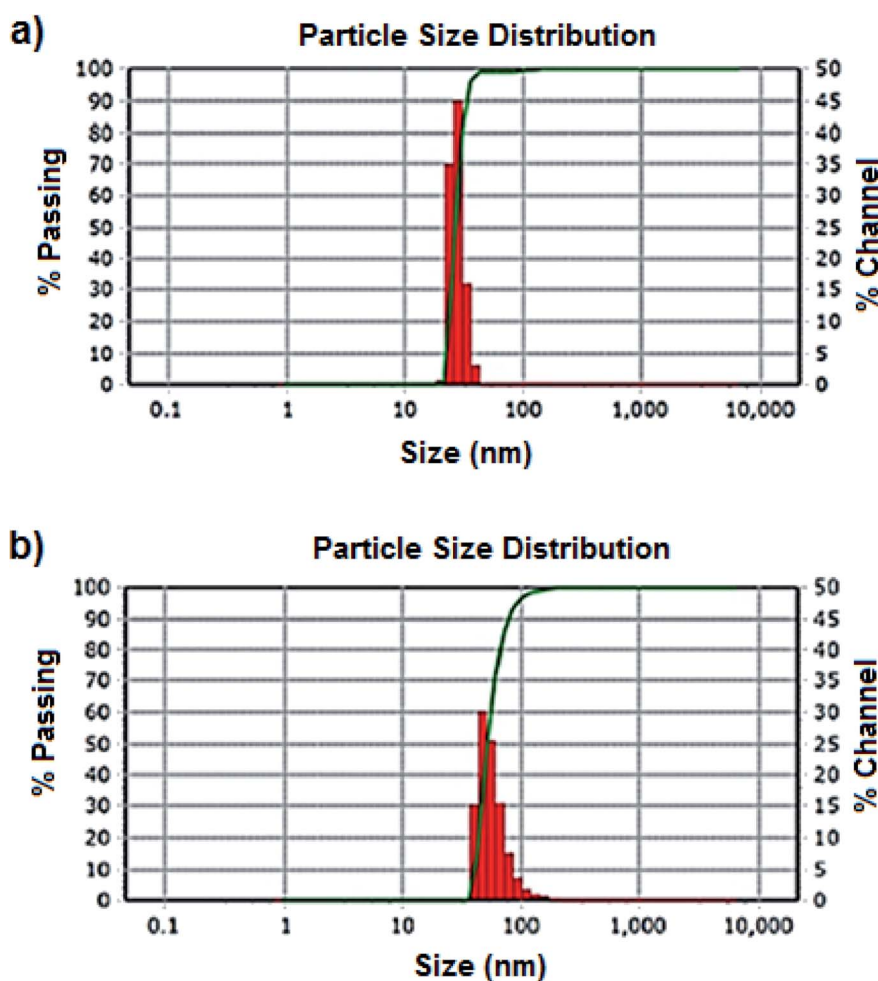


Fig. 1 (a) Size distribution of nearly monodisperse Fe<sub>3</sub>O<sub>4</sub> NPs, with an average hydrodynamic diameter of 26.9 nm ± 7. (b) Size distribution of silanized Fe<sub>3</sub>O<sub>4</sub> NPs, with an average hydrodynamic diameter of 52.7 nm ± 3. Hydrodynamic diameters are in the appropriate range for biomedical uses.



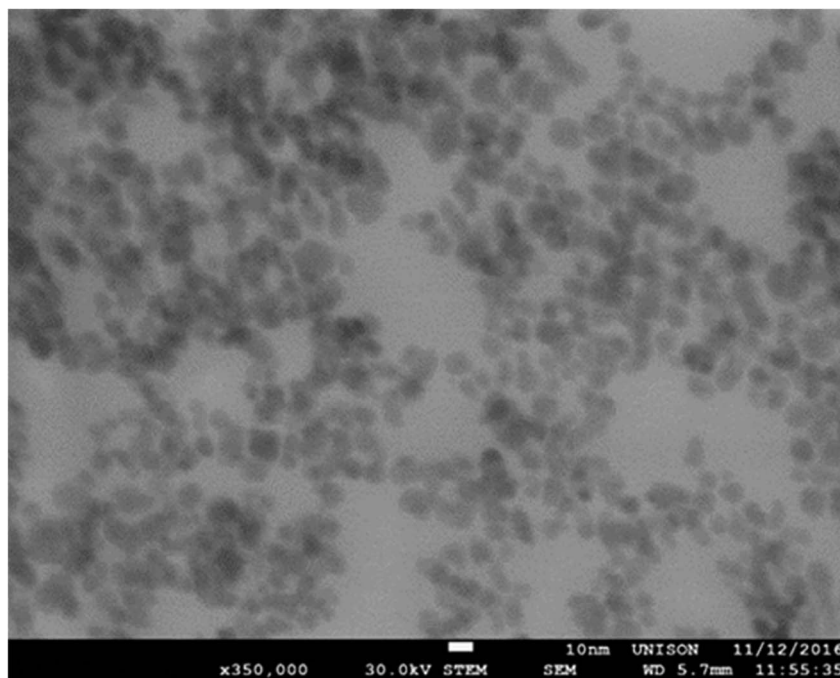


Fig. 2 Nearly spherical  $\text{Fe}_3\text{O}_4$  nanoparticles of approximately  $12 \text{ nm} \pm 4$  as observed by scanning transmission electron microscopy (STEM).

**Recognition of the secondary antibody conjugate ( $\text{Fe}_3\text{O}_4$  NPs – Ab).** 100.0  $\mu\text{L}$  of the  $\text{Fe}_3\text{O}_4$  NPs – Ab conjugate were placed in each well for its interaction with NS1. The plates were incubated at room temperature for 1 hour. At the end of the incubation period, washes were made with PBS 1X.<sup>26</sup>

**Plate revelation.** The plate was revealed using the Perls' Prussian blue staining protocol, which is a staining technique developed for detecting exogenous  $\text{Fe}^{3+}$  ions on tissues and solutions. Since the NPs of magnetite are composed of  $\text{Fe}^{2+}$  and  $\text{Fe}^{3+}$  ions, the use of potassium ferrocyanide (Perls reagent) in

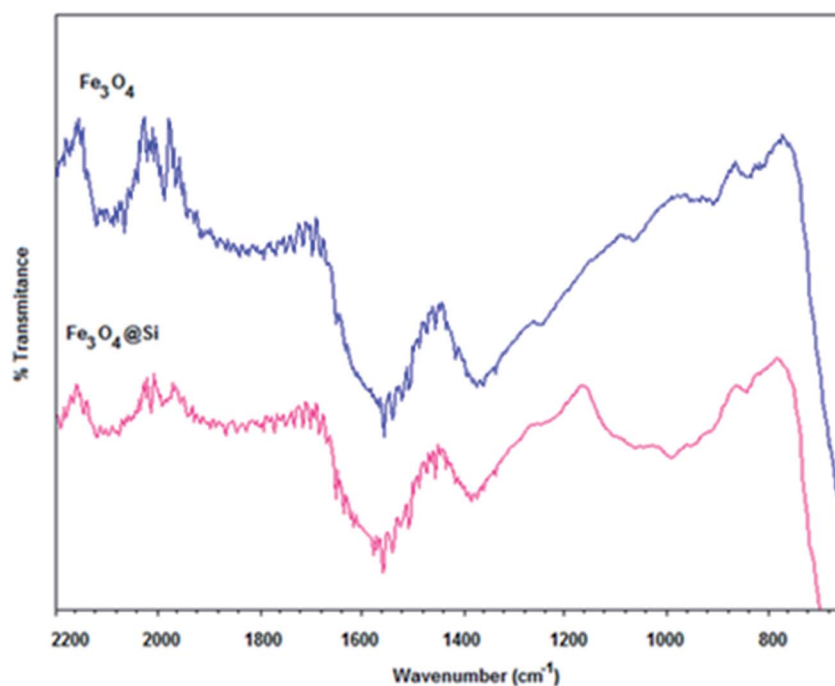


Fig. 3 FTIR spectra of  $\text{Fe}_3\text{O}_4$  NPs (blue) and silanized  $\text{Fe}_3\text{O}_4@\text{SiO}_2$  NPs. The vibrational band at  $590 \text{ cm}^{-1}$ , corresponding to the Fe–O stretching, is well defined in both spectra, as well as the band at  $1100 \text{ cm}^{-1}$  corresponding to Si–O–Fe stretching in the surface silanized nanoparticles.



the presence of NPs yields a blue, insoluble, iron complex. Therefore, the Perls reagent would interact with the  $\text{Fe}_3\text{O}_4$  NPs present in the secondary antibody conjugate coupled in the plate. For this, 100.0  $\mu\text{L}$  of the solution was added to each well and incubated for 30 minutes at room temperature. The blue color change was visible to the naked eye. In order to make an accurate determination of the colorimetric change, the intensity of the color was measured at 450 nm with a Multiskan MCC/340, Thermo Fisher Scientific.<sup>27–29</sup> The data were analyzed with the Kruskal–Wallis test ( $P < 0.0001$ ); in addition, a Dunn multiple comparison test was performed.

## Results and discussion

### Synthesis and characterization of magnetite nanoparticles

**Size.** The particle size distribution analysis determined an average size of  $26.9 \text{ nm} \pm 8.0$ , with a monodisperse population, which was within the range expected for the study (Fig. 1a). It has been previously reported that magnetic NPs with diameters between 1 and 100 nm were appropriate for biomedical applications. In addition, their surface-volume ratio is inversely proportional to their diameter, so that the lower their volume, the greater the surface area, compared to macroscopic materials.<sup>14,30–35</sup> Because of this, the nanoparticles may present a large number of attachment sites on their surface that can be used for chemical functionalization. In this work, this feature was used to attach an aminosilane derivative to the NP surface which was then used for covalently binding the NS1 antibody to form the magnetic immunoconjugated nanoplatform. The DLS analysis of the modified NPs (Fig. 1b) indicated that the average size of the antibody-conjugated NPs was  $52.7 \text{ nm} \pm 3.0$ , with a monodisperse population, still being within the ranges required for biomedical uses.

**Morphology.** Analysis by STEM revealed that the unmodified NPs were nearly spherical and of approximately  $12 \text{ nm} \pm 4.0$  (Fig. 2), which is in agreement with the results obtained by DLS. Stephen and collaborators (2011) mentioned that magnetic NPs  $< 20 \text{ nm}$  have higher magnetization and remanence equal to zero (superparamagnetism), this being a useful property and a desirable characteristic for biomedical applications.<sup>13</sup>

**Chemical modification.** The FTIR analysis clearly showed the characteristic vibrational bands associated with the expected functional groups on the surface of the material, such as the Fe–O stretching vibration at  $580 \text{ cm}^{-1}$  and their interactions with water. Likewise, as previous studies have reported, this analysis

helped to evaluate the degree of silanization of the nanoparticles. The vibrational band around  $1100 \text{ cm}^{-1}$ , corresponding to the Si–O–Fe stretching vibration, is indicative of successful APTMS functionalization of the nanoparticle surface.<sup>21,36</sup> The vibrational spectra are shown in Fig. 3. The outer shell of the chemically modified  $\text{Fe}_3\text{O}_4$  NPs was composed of silane groups with amine ( $-\text{NH}_2$ ) terminations. This functionalization improved the stability for the magnetic NPs in solution, avoiding agglomeration, since the partial surface charges of vicinal NPs repel each other.<sup>19</sup> In addition, the amino terminal group gives the NPs the ability to covalently bind the anti-NS1 antibody by coupling through the end-terminal carboxyl ( $-\text{COOH}$ ) groups.

### NS1 protein production

**Quantification of the total protein.** It was analyzed by the Bradford method, in which both the infected supernatant and

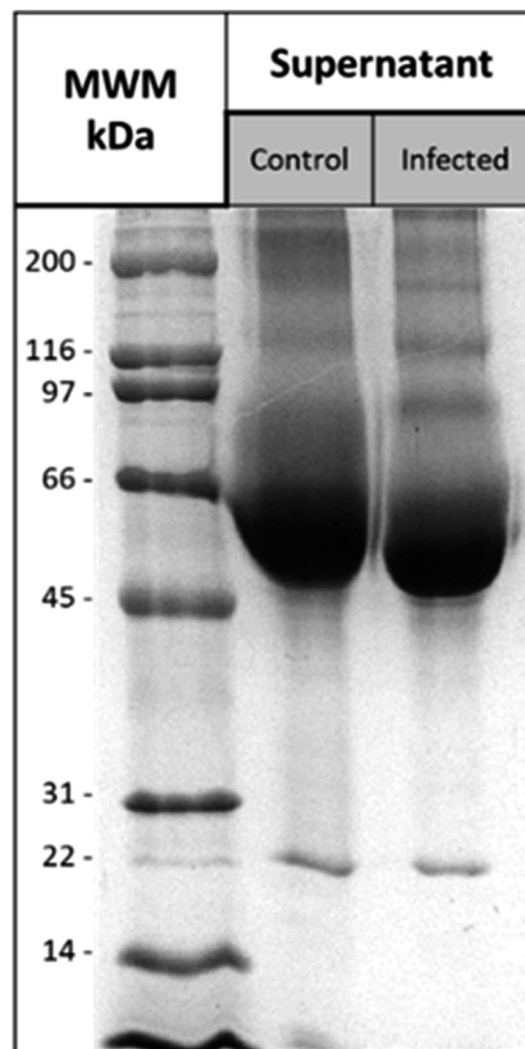


Fig. 4 Polyacrylamide gel electrophoresis of supernatants U937-DC-SIGN. The electrophoretic profile of the supernatants is shown. Lines 1, 2 and 3 correspond to the molecular weight marker (MWM), the control supernatant and the infected supernatant, respectively.

Table 1 Quantification of total proteins in supernatants of U937-DC-SIGN cells

Supernatant	Concentration $\mu\text{g mL}^{-1}$
Infected	3544.9
Control	3190.3
Difference <sup>a</sup>	354.6

<sup>a</sup> Total protein production and detection of the NS1 protein by SDS-PAGE.



the control supernatant were analyzed, which showed a total protein concentration of  $3544.9 \mu\text{g mL}^{-1}$  and  $3190.26 \mu\text{g mL}^{-1}$  respectively. The difference between the protein concentrations of both supernatants was  $354.6 \mu\text{g mL}^{-1}$ , and this value would correspond to the NS1 protein (Table 1). Therefore, once the protein content was estimated, the successive tests were carried out.

The electrophoretic profile of the supernatants of the infected and control cell line cultures is shown in Fig. 4. A band of approximately 91 kDa in the infected supernatant was observed and differs from that of the control profile. This band would correspond to the NS1 protein dimer. The NS1 protein has an approximate weight of 48 kDa, but in its native form it exists as a dimer of approximately 96 kDa. The dimer is the typical structure of NS1 found in the extracellular medium. Therefore, the presence of this band corroborated the presence of this protein in the supernatant, which would be used in our study.<sup>37–39</sup>

Then, a densitometry analysis was performed for the 91.6 kDa band, which presented a band density of 3.7%. Considering the total protein content, the amount of the equivalent protein was estimated, obtaining a concentration of  $131.16 \mu\text{g mL}^{-1}$ , which would correspond to the concentration of the NS1 protein present in the supernatant as a dimer.

### Nanoplatfom design for the detection of the NS1 protein

**System evaluation.** The immunodetection of the NS1 protein of dengue virus was carried out by the formation of the immunoconjugate, as shown in Fig. 5. A color change, produced by the reaction of formation of a Prussian blue precipitate, was observed just in the wells where the protein was present after it conjugated to the magnetic nanoplatfom. This immunodetection is visible because the Perl's reagent contains potassium ferrocyanide which interacts with the iron(III) ions that are a part of the chemical composition of the magnetic nanoparticles conjugated to the protein, which are also conjugated to the immobilized second antibody in the well. The formation of a ferric ferrocyanide precipitate turns the corresponding well blue. It was observed that the color intensity was proportional to the amount of antibody Ab41616 coupled to the NPs, where at  $1.41 \mu\text{g mL}^{-1}$  the well showed a significant intensity that was possible to detect even by the naked eye, as shown in the first row of Fig. 5a. Likewise, as is presented in Fig. 5b, in the second row of the plate no precipitate formed when other antibodies were used (Anti-Mouse, Goat pAb to Ms IgG (HRP) Ab97023 Lot: GR45780-7, abcam), which indicates that this system did not generate complexes when an irrelevant antibody is used even when the NS1 protein and the NPs were present.

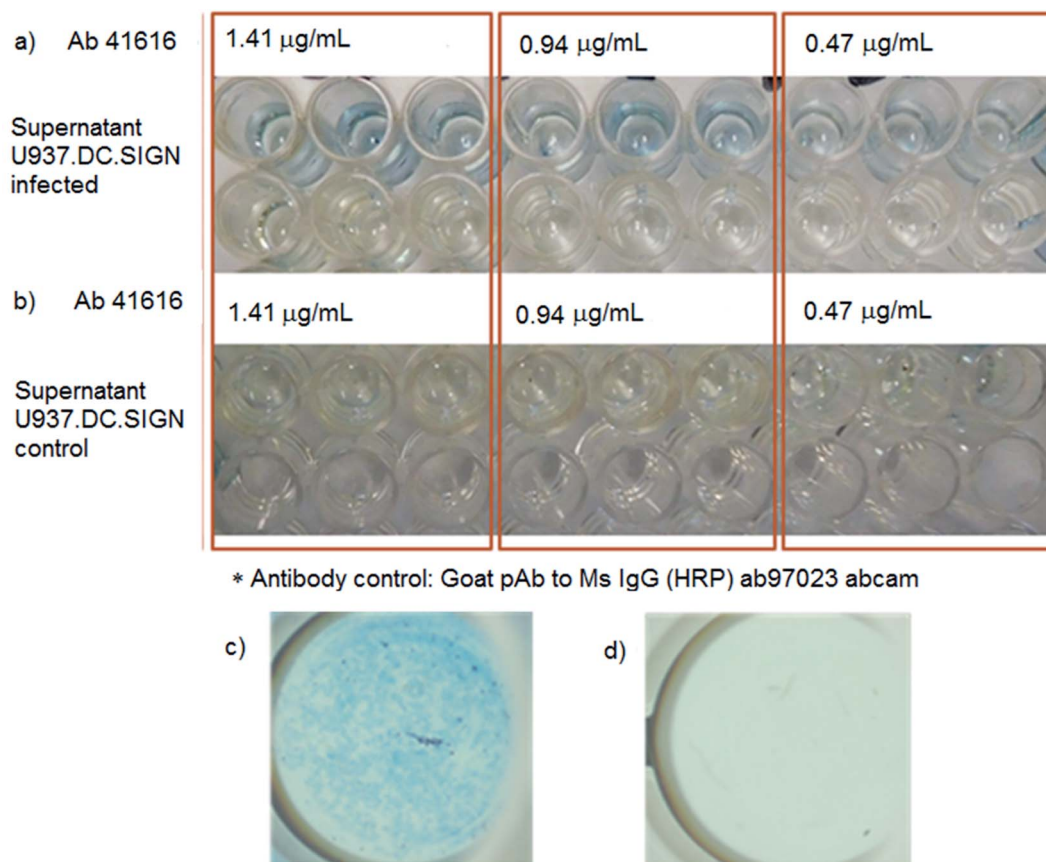


Fig. 5 Evaluation of the immunoconjugate performance toward the detection of the NS1 protein. (a) Positive result as evidenced by the color change (Perls reaction). (b) Negative result in the absence of the protein. (c) Formation of a blue ferric ferrocyanide precipitate as evidence of the immunoconjugate formation; (d) no blue precipitate is generated in the absence of the NS1 protein.



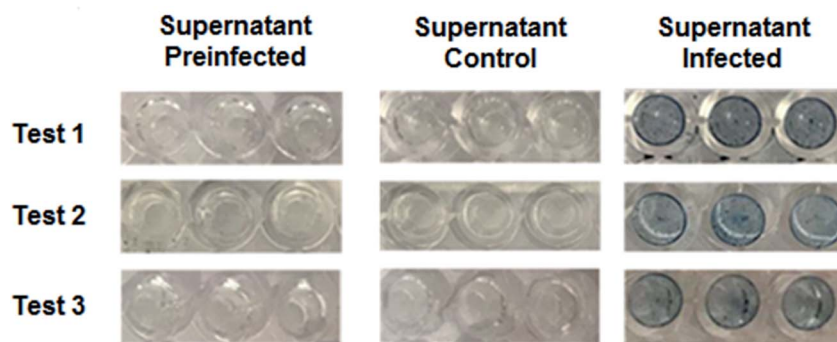


Fig. 6 Qualitative evaluation of the reproducibility of the immunodetection assay of the NS1 protein. The triplicates of the assays are presented, where immunodetection of the protein is observed in all the wells of the infected supernatant. Likewise, there was no change in the pre-infected supernatant and control wells.

When the protein is absent, as shown in Fig. 5b, no color change was observed which suggests that the immunocomplex nanoplateform-antibody does not interact with the plate in the absence of recognition of the specific protein, confirming that no false positives were produced in this test. In addition, a magnification of the wells of the plate was carried out, to corroborate the presence of precipitated iron ferrocyanide deposits as a result from the immunodetection of the virus protein (Fig. 5c), evidencing the specific wells where the NS1 protein was detected. A magnification in a well where the irrelevant antibody coupled to the NPs was used showed no formation of precipitates even when the NS1 protein was present, reinforcing the detection capabilities of the present method (Fig. 5d).

**Reproducibility of the system.** After the optimal conditions for the system were established, the reproducibility of the assay was assessed. As shown in Fig. 6, the immunodetection of the NS1 protein of dengue virus was carried out efficiently using the infected supernatants (tested in triplicate). The characteristic color change could be observed with the naked eye. In contrast, in the wells with supernatants of the pre-infected serum and control, no color change was observed, in agreement with no false positive production in the system.

Likewise, to obtain a quantitative result, the data obtained from these tests were analyzed by absorbance measurement at 450 nm. The data obtained in the assays of absorbance measurements are presented in Table 2. In addition, these data were plotted according to their absorbance (Fig. 7), where

a notable difference is observed in the infected supernatants compared to the controls, with reproducible values. These data were corroborated by statistical analysis, where the infected supernatant presents a statistically significant difference with a  $P < 0.0001$ , as indicated by the Kruskal-Wallis test, on the control supernatants. In addition, a Dunn multiple comparison test was performed, in which it was observed that there was a statistically significant difference ( $P < 0.0001$ ) between the infected supernatant and the pre-infected supernatant. Likewise, a statistical difference with a  $P < 0.01$  between the infected supernatants and control was observed. However, in the case of the comparison between pre-infected supernatants and control supernatants, no statistically significant difference was observed ( $P > 0.05$ ), which is because in both cases none of them presents the protein. The same result was obtained both by qualitative and quantitative tests. The range of the concentration of NS1 that this system was able to detect was calculated to be in the range from 0.415 to 1.24  $\mu\text{g mL}^{-1}$ , considering the concentration of the  $\text{Fe}_3\text{O}_4$  NPs-Ab41616 conjugate used to detect NS1 (0.47–1.41  $\mu\text{g mL}^{-1}$ ).

Finally, in order to determine the affordability of the developed diagnostic test, the cost of a single test was calculated to be around one dollar per sample, considering all the involved expenses (reagents, disposable materials, solvents). This low cost is affordable and competitive in comparison with that of other commercially available detection technologies, and makes this a new method of interest due to its low economic impact, accelerating the development of first line diagnostic

Table 2 Immunodetection assay data of the NS1 protein in the supernatants of U937-DC-SIGN cells

	Test 1			Test 2			Test 3		
	1	2	3	1	2	3	1	2	3
Supernatant Preinfected	0.068	0.070	0.067	0.068	0.070	0.065	0.063	0.069	0.065
Supernatant Control	0.070	0.070	0.070	0.073	0.071	0.069	0.071	0.072	0.073
Supernatant Infected	0.128	0.134	0.122	0.123	0.170	0.140	0.158	0.142	0.133



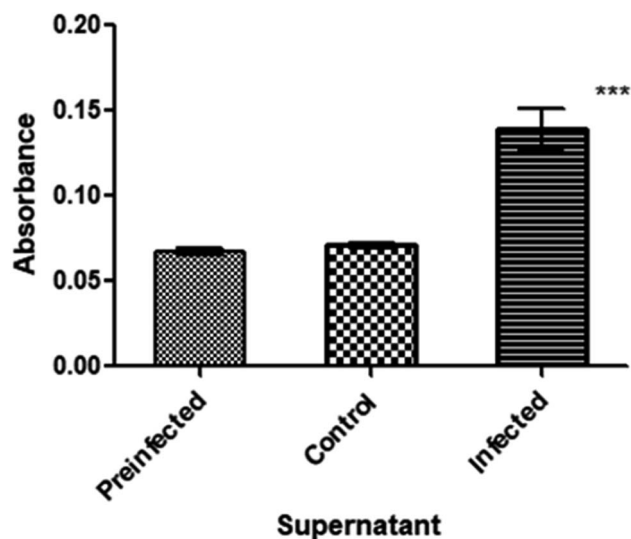


Fig. 7 Reproducibility test of the immunoconjugate system. Absorbance of NS1 protein detection assays, where the infected supernatant presents a statistically significant difference ( $P < 0.001$ ), as indicated by the Kruskal–Wallis test.

kits for the determination of viral infection, with a minimal and simple experimental setup.<sup>40</sup> For example, the gold standard method for dengue detection is performed in centralized laboratories, using large automated clinical analyzers for nucleic acids or microarrays. Other methods, regularly, need more or less complex pre-treatment of the sample in order to concentrate, extract or purify the NS1 protein that will be detected. In addition, commercially available methods require complex and expensive instrumentation such as electrochemical workstations, LCR meters, microcentrifuges, fluorescence or visible plate reader spectrophotometers for ELISA tests, or Raman spectrometers and expensive reagents (fluorescent dyes, protein chromatographic columns, commercial beads or nanoparticles). They are the quite significant differences with respect to the diagnostic method reported here. In this sense, the present colorimetric system could become accessible for remote, rural and increasingly urban communities and it could be incorporated into commercial antibody detection kits avoiding the requirement of highly trained staff, time-consuming delays, accelerating the acquisition of results and decreasing the high costs associated with the clinical tests.

## Conclusions

In the present work, a novel approach for the detection of biomolecules associated with viral infection, in this specific case, the diagnosis of dengue virus infection based on the colorimetric detection of the NS1 protein using magnetic nanoparticles conjugated with NS1 antibodies, is presented. The detection could be evidenced by a simple and cheap, naked eye perceptible, blue color change produced by the Perl's reaction. The potential of the magnetite nanoconjugates for the colorimetric detection of the NS1 protein was successfully evaluated. It was observed that the immunoconjugate was able

to perform a colorimetric detection of the NS1 protein of dengue virus, after magnetic separation from the infected serum, formation of an immunoconjugate sandwich complex followed by a color change after Perl's staining. This colorimetric system could be applied in remote and rural areas of cities with limited access to expensive and complex analytical tools or facilities for dengue diagnosis such as those usually available at medical laboratories where ELISA tests have become an everyday analytical method. Future work will focus on reducing the current limitations of the detection method, as well as optimizing the sensitivity and discrimination ability against potential interference. Evaluation of the performance of this method for the detection of other emerging viral infections is currently under consideration.

## Abbreviations

NPs	Nanoparticles
Fe <sub>3</sub> O <sub>4</sub> NPs	Magnetite nanoparticles
Fe <sub>3</sub> O <sub>4</sub> @Si	Silanized magnetite nanoparticles
DLS	Dynamic light scattering
STEM	Scanning transmission electron microscopy
FT-IR	Fourier-transform infrared spectroscopy
DENV	Dengue virus
NS1	Nonstructural protein
MOI	Multiplicity of infection
SFB	Serum fetal bovine
APTMS	Aminopropyl trimethoxysilane

## Author contributions

RRN performed experimental work and interpretation of the results. PP performed experimental work and interpretation of the results. JRL designed experiments and analyzed and discussed the results. UH discussed the results. JCVC discussed the results. MPM designed experiments, analyzed and discussed the results and wrote the paper. MAMR designed experiments, analyzed and discussed the results, and wrote the paper. AAM designed experiments, analyzed and discussed the results and wrote the paper.

## Funding sources

This work was partially supported by red PRODEP 2016, Project: Nanotechnology as a tool for the Diagnosis and Treatment of Infectious Diseases and by CONACYT (Grants # CB-2010/154602 and INFR-2014/02-23053). Partial support from the Office of Graduate Studies and Research (UDLAP) and CIBIOR is acknowledged.

## Conflicts of interest

There are no conflicts to declare.





## Acknowledgements

The authors are thankful to Adriana Garibay and Alejandro Tapia Gonzalez for their useful suggestions on the manuscript. Technical support of Tania C. Hidalgo-Castillo and Andrea Diaz-Gaxiola (UDLAP), Carolina Jasso and Lilian K. Flores (Laboratory of Immunology and Virology, CIBIOR) and technical support of Biophysics Laboratory-DIFUS, Nanotechnology Laboratory are deeply acknowledged. JRL acknowledges support of Fundación IMSS.

## References

- 1 N. Khetarpal and I. Khanna, Dengue Fever: Causes, Complications, and Vaccine Strategies, *J. Immunol. Res.*, 2016, **2016**, 6803098.
- 2 CDC. Center for Disease Control and Prevention, *Dengue-Statistic and Maps-2020*, available in <https://www.cdc.gov/dengue/index.html>.
- 3 J. Ramos-Castañeda, F. Barreto dos Santos, R. Martínez-Vega, J. M. Galvão de Araujo, G. Joint and E. Sarti, Dengue in Latin America: Systematic Review of Molecular Epidemiological Trends, *PLoS Neglected Trop. Dis.*, 2017, **11**(1), 1–24.
- 4 S. de Salud, Panorama Epidemiológico de Dengue, 2020, Sem. Epidemiol. 11, 2020, 16 de Marzo, Gobierno de México, available in: [https://www.gob.mx/cms/uploads/attachment/file/542111/Pano\\_dengue\\_11\\_2020.pdf](https://www.gob.mx/cms/uploads/attachment/file/542111/Pano_dengue_11_2020.pdf).
- 5 World Health Organization, *Handbook for Clinical Management of Dengue*, WHO, Switzerland, 7th edn, 2012.
- 6 L. Guo, S. Xu, X. Ma, B. Qiu, Z. Lin and G. Chen, Dual-Color Plasmonic Enzyme-Linked Immunosorbent Assay Based on Enzyme-Mediated Etching of Au Nanoparticles, *Sci. Rep.*, 2016, **6**(9), 1–7.
- 7 S. I. De la Cruz-Hernández, H. Flores-Aguilar, S. González-Mateos, I. López-Martínez, C. Alpuche-Aranda, J. E. Ludert and R. M. del Angel, Determination of viremia and concentration of circulating nonstructural protein 1 in patients infected with dengue virus in Mexico, *Am. J. Trop. Med. Hyg.*, 2013, **88**(3), 446–454.
- 8 T. V. Tran, B. V. Nguyen, T. T. P. Nguyen, T. T. Tran, K. G. Pham, Q. B. Le, B. N. Do, H. N. Pham, C. V. Nguyen, D. P. H. Dinh, V. T. Ha, T. H. T. Doan and H. Q. Le, Development of a highly sensitive magneto-enzyme lateral flow immunoassay for dengue NS1 detection, *PeerJ*, 2019, **7**, e7779.
- 9 P. Antunes, D. Watterson, M. Parmvi, R. Burger, A. Boisen, P. Young, M. A. Copper, M. F. Hansen, A. Ranzoni and M. Donolato, Quantification of NS1 dengue biomarker in serum via optomagnetic nanocluster detection, *Sci. Rep.*, 2015, **5**, 16145.
- 10 S. Alcon, A. Talarmin, M. Debruyne, A. Falconar, V. Deubel and M. Flamand, Enzyme-linked immunosorbent assay specific to dengue virus type 1 nonstructural protein NS1 reveals circulation of the antigen in the blood during the acute phase of disease in patients experiencing primary or secondary infections, *J. Clin. Microbiol.*, 2002, **40**(2), 376–381.
- 11 J. J. Valdez-Sandoval, D. Ruiz-Amores, S. C. Vázquez-Ramudo, N. Calzada-Gutiérrez and C. M. G. Guzmán-Tirado, Evaluación Del Sistema Diagnóstico SD Dengue Duo Para La Detección de La Proteína NS1 Y Los Anticuerpos IgM E IgG Anti-Dengue, *Rev. Cubana Med. Trop.*, 2012, **64**(1), 27–34.
- 12 M. Namekar, E. M. Ellis, M. O'Connell, J. Elm, A. Gurary, S. Y. Park, A. Imrie and V. R. Nerurkar, Evaluation of a New Commercially Available Immunoglobulin M Capture Enzyme-Linked Immunosorbent Assay for Diagnosis of Dengue Virus Infection, *J. Clin. Microbiol.*, 2013, **51**(9), 3102–3106.
- 13 Z. R. Stephen, F. M. Kievit and M. Zhang, Magnetite Nanoparticles for Medical MR Imaging, *Mater. Today*, 2011, **14**(7–8), 330–338.
- 14 J. Lim, S. P. Yeap, H. X. Che and S. C. Low, Characterization of Magnetic Nanoparticle by Dynamic Light Scattering, *Nanoscale Res. Lett.*, 2013, **8**(1), 1–14.
- 15 X. Li, H. Kong, R. Mout, K. Saha, D. F. Moyano, S. M. Robinson, S. Rana, X. Zhang, M. A. Riley and V. M. Rotello, Rapid Identification of Bacterial Bio Films and Bio Film Wound Models Using a Multichannel Nanosensor, *ACS Nano*, 2014, **8**(12), 12014–12019.
- 16 T. Lu, H. Lee, T. Chen, S. Herchak, J.-H. Kim, S. E. Fraser, R. C. Flagan and K. Vahala, High Sensitivity Nanoparticle Detection Using Optical Microcavities, *Proc. Natl. Acad. Sci. U. S. A.*, 2011, **108**(15), 5976–5979.
- 17 Y. Zhang and J. Zhang, Surface Modification of Monodisperse Magnetite Nanoparticles for Improved Intracellular Uptake to Breast Cancer Cells, *J. Colloid Interface Sci.*, 2005, **283**(2), 352–357.
- 18 S. Qu, H. Yang, D. Ren, S. Kan, G. Zou, D. Li and M. Li, Magnetite Nanoparticles Prepared by Precipitation from Partially Reduced Ferric Chloride Aqueous Solutions, *J. Colloid Interface Sci.*, 1999, **215**(1), 190–192.
- 19 K. Li, M. Shen, L. Zheng, J. Zhao, Q. Quan, X. Shi and G. Zhang, Magnetic Resonance Imaging of Glioma with Novel APTS-Coated Superparamagnetic Iron Oxide Nanoparticles, *Nanoscale Res. Lett.*, 2014, **9**(1), 1–11.
- 20 F. Arteaga-Cardona, E. Gutiérrez-García, S. Hidalgo-Tobón, C. López-Vasquez, Y. A. Brito-Barrera, J. Flores-Tochihuitl, A. Angulo-Molina, J. R. Reyes-Leyva, R. González-Rodríguez, J. L. Coffey, *et al.*, Cell viability and MRI performance of highly efficient polyol-coated magnetic nanoparticles, *J. Nanopart. Res.*, 2016, **18**(11), 345.
- 21 A. Angulo-Molina, M. Á. Méndez-Rojas, T. Palacios-Hernández, O. E. Contreras-López, G. A. Hirata-Flores, J. C. Flores-Alonso, S. Merino-Contreras, O. Valenzuela, J. Hernández and J. Reyes-Leyva, Magnetite nanoparticles functionalized with  $\alpha$ -tocopheryl succinate ( $\alpha$ -TOS) promote selective cervical cancer cell death, *J. Nanopart. Res.*, 2014, **16**(8), 2528.
- 22 F. Arteaga-Cardona, E. Santillán-Urquiza, P. de la-Presa, S. Hidalgo-Tobón, P. Umapada, P. Horta-Fraijo, M. J. Yacamán, J. D. Lozada-Ramírez, R. Ivkov, A. Angulo-Molina, *et al.*, Enhanced Magnetic Properties and MRI



- Performance of Bi-Magnetic Core-shell Nanoparticles, *RSC Adv.*, 2016, **6**(81), 77558–77568.
- 23 E. Orna and Z. Tsaffrir, Linearization of the Bradford Protein Assay, *J. Visualized Exp.*, 2010, **38**, 1–6.
- 24 U. K. Laemmli, Cleavage of Structural Proteins during the Assembly of the Head of Bacteriophage T4, *Nature*, 1970, **227**(5259), 680–685.
- 25 A. Sassolas, L. J. Blum and B. D. Leca-Bouvier, Immobilization Strategies to Develop Enzymatic Biosensors, *Biotechnol. Adv.*, 2012, **30**(3), 489–511.
- 26 C.-W. Yen, H. de Puig, J. Tam, J. Gómez-Márquez, I. Bosch, K. Hamad-Schifferli and L. Gehrke, Multicolored Silver Nanoparticles for Multiplexed Disease Diagnostics: Distinguishing Dengue, Yellow Fever, and Ebola Viruses, *Lab Chip*, 2015, **15**(7), 1638–1641.
- 27 M. S. U. Ahmed, A. B. Salam, C. Yates, K. Willian, J. Jaynes, T. Turner and M. O. Abdalla, Double-Receptor-Targeting Multifunctional Iron Oxide Nanoparticles Drug Delivery System for the Treatment and Imaging of Prostate Cancer, *Int. J. Nanomed.*, 2017, **12**, 6973–6984.
- 28 K. Dobretsov, S. Stolyar and A. Lopatin, Magnetic Nanoparticles: A New Tool for Antibiotic Delivery to Sinonasal Tissues. Results of Preliminary Studies, *Acta Otorhinolaryngol Ital*, 2015, **35**(2), 97–102.
- 29 S. Leekha, A. Nayar, P. Bakshi, A. Sharma, S. Parhar and S. Soni, Estimation of Iron Overloads Using Oral Exfoliative Cytology in Beta-Thalassemia Major Patients, *Cytojournal*, 2016, **13**(1), 6.
- 30 R. Hufschmid, H. Arami, R. M. Ferguson, M. Gonzales, L. N. Brush, N. D. Browning, K. M. Krishnan, C. S. Directorate and P. Northwest, Synthesis of Phase-Pure and Monodisperse Iron Oxide Nanoparticles by Thermal Decomposition, *Nanoscale*, 2016, **7**(25), 11142–11154.
- 31 Y. Xie, D. Liu, C. Cai, X. Chen, Y. Zhou, L. Wu, Y. Sun, H. Dai, X. Kong and P. Liu, Size-Dependent Cytotoxicity of Fe<sub>3</sub>O<sub>4</sub> Nanoparticles Induced by Biphasic Regulation of Oxidative Stress in Different Human Hepatoma Cells, *Int. J. Nanomed.*, 2016, **11**, 3557–3570.
- 32 M. R. Ghazanfari, M. Kashefi, S. F. Shams and M. R. Jaafari, Perspective of Fe<sub>3</sub>O<sub>4</sub> Nanoparticles Role in Biomedical Applications, *Biochem. Res. Int.*, 2016, **2016**, 32.
- 33 M. Bloemen, W. Brullot, T. T. Luong, N. Geukens, A. Gils and T. Verbiest, Improved Functionalization of Oleic Acid-Coated Iron Oxide Nanoparticles for Biomedical Applications, *J. Nanopart. Res.*, 2012, **14**(9), 1–10.
- 34 A. Lassenberger, T. A. Grünwald, P. D. J. Van Oostrum, H. Rennhofer, H. Amenitsch, R. Zirbs, H. C. Lichtenegger and E. Reimhult, Monodisperse Iron Oxide Nanoparticles by Thermal Decomposition: Elucidating Particle Formation by Second-Resolved in Situ Small-Angle X-Ray Scattering, *Chem. Mater.*, 2017, **29**(10), 4511–4522.
- 35 R. R. Shah, T. P. Davis, A. L. Glover, D. E. Nikles and C. S. Brazel, Impact of Magnetic Field Parameters and Iron Oxide Nanoparticle Properties on Heat Generation for Use in Magnetic Hyperthermia Rhythm, *J. Magn. Magn. Mater.*, 2015, **387**(205), 96–106.
- 36 M. Mahdavi, M. B. Ahmad, M. J. Haron, F. Namvar, B. Nadi, M. Z. Ab Rahman and J. Amin, Synthesis, Surface Modification and Characterisation of Biocompatible Magnetic Iron Oxide Nanoparticles for Biomedical Applications, *Molecules*, 2013, **18**(7), 7533–7548.
- 37 P. Avirutnan, A. Fuchs, R. E. Hauhart, P. Somnuke, S. Youn, M. S. Diamond and J. P. Atkinson, Antagonism of the Complement Component C4 by Flavivirus Nonstructural Protein NS1, *J. Exp. Med.*, 2010, **207**(4), 793–806.
- 38 M. Flamand, F. Megret, M. Mathieu, J. Lepault, F. Rey and V. Deubel, Dengue Virus Type 1 Nonstructural Glycoprotein NS1 Is Secreted from Mammalian Cells as a Soluble Hexamer in a Glycosylation-Dependent Fashion, *J. Virol.*, 1999, **73**(7), 6104–6110.
- 39 I. Gutsche, F. Coulibaly, J. E. Voss, J. Salmon, J. d'Alayer, M. Ermonval, E. Larquet, P. Charneau, T. Krey, F. Megret, *et al.*, Secreted Dengue Virus Nonstructural Protein NS1 Is an Atypical Barrel-Shaped High-Density Lipoprotein, *Proc. Natl. Acad. Sci. U. S. A.*, 2011, **108**(19), 8003–8008.
- 40 Y. Saylan, Ö. Erdem, S. Ünal and A. Denizli, An Alternative Medical Diagnosis Method: Biosensors for Virus Detection, *Biosensors*, 2019, **9**(2), 65.

